Identifying, characterizing and understanding Nefiracetam solid state forms: a potential antidementia drug

Xavier Buol [a, *], Koen Robeyns [a], Nikolay Tumanov [b], Johan Wouters [b] and Tom Leyssens [a, *]

[a]Institute of Condensed Matter and Nanosciences, UCLouvain, 1 Place Louis Pasteur, B-1348 Louvain-la-Neuve, Belgium

[b]Unité de Chimie Biologique et Structurale, Chemistry Department, UNamur, 61 rue de Bruxelles, B-5000 Namur, Belgium

ABSTRACT

In this work, three hitherto unidentified solid-state forms of the nootropic drug Nefiracetam are identified: a monohydrate and two polymorphic phases of the anhydrate. These new forms were investigated from a structural and thermodynamic point of view to evaluate the possibility of using these forms in alternative formulations. Furthermore, their dissolution rate and solubility were compared.

INTRODUCTION

Hampering mental function decline is one of the pathways to battle dementia (Alzheimer or cerebrovascular dementia)[1-4]. Cognitive-enhancers or nootropic agents have been developed to treat people with cerebral deficiencies (dementia or Alzheimer) that could occur due to a reduction of y-aminobutyric acid (GABA) in the brain. GABA therefore forms the basic guide to the development of nootropic agents. Nefiracetam (N-(2,6-dimethylphenyl)-2-(2-oxopyrrolidin-1-yl)acetamide) known under the label DM-9384 or Motiva/Translon is such an agent (**Figure 1**). Being a pyrolidone derivative, Nefiracetam was produced and developed during the 90's by Daiichi Sankyo and marketed in 2002 in Japan[5]. Animal based studies suggest three main biological effects of DM-9384: a neurotransmitters release through Ca^{2+} channel activation[6], an impact on the GABAergic/monoaminergic/cholinergic systems and an enhancement of the protein metabolism in the brain[7-9]. *In vitro* and *in vivo* toxicity studies did not show any mutagenic[10], antigenic[11], oncogenic or teratogenic[12] effects in laboratory animals. Nowadays, Nefiracetam is still commercially available and administered to people with cognitive issues.

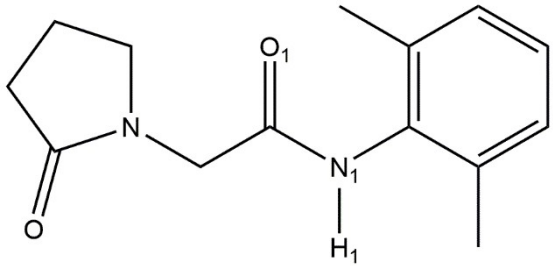

Figure 1: Molecular diagram of Nefiracetam (*N*-(2,6-dimethylphenyl)-2-(2-oxopyrrolidin-1-yl)acetamide).

Due to increasing molecular complexity, 75% of all new chemical entities show low water solubility and high permeability (BCS class II) or low water solubility and low permeability (BCS class IV). [13-14] Nefiracetam (BCS class II) [15-16] is part of the low water solubility compounds. As a consequence, the oral absorption and overall bioavailability of this molecule are low[17]. For compounds such as Nefiracetam, formulation tools need to be applied to increase their bioavailability [18-19]. One such solution is the use of an alternative solid phase showing a higher solubility or dissolution rate, such as the amorphous phase, metastable forms, polymorphic forms, salts (not applicable here), hydrates/solvates or cocrystals[20-25]. In this study, we set out to identify new solid-state forms of Nefiracetam, and to study the potential of these forms as alternative formulation candidates. Up to now, only one single solid state form of Nefiracetam has been identified and characterized. Wang et al[26] described an anhydrous form, which we will refer to as Form I (**FI**). Here, we identify two hitherto unknown polymorphs (**FII** and **FIII**) of this anhydrate as well as a hydrate form. All forms were structurally analyzed, their stability relationship studied, and their dissolution profiles compared.

MATERIAL AND METHODS

Materials

Nefiracetam was sourced from Xiamen Top Health. All solvents used are commercially available from VWR. Solvents were used as received without any additional purification. Nefiracetam was purified by slurrying the compound overnight in ethyl acetate at room temperature after which the suspension was filtered and dried.

Form screening

Evaporative experiments were performed by dissolving 0.1 mmol of Nefiracetam in a suitable amount of solvent in order to prepare undersaturated solution. Solutions were then left to evaporate (over periods ranging from 3 to 7 days) at room temperature, and solid phases retrieved.

Cooling experiments were performed by preparing supersaturated Nefiracetam solutions. An excess amount of Nefiracetam was added to a given solvent at room temperature, and vials placed at 50°C to achieve full dissolution. They were then stored at -15°C or alternatively at 9°C for three days. Solid phases were retrieved and analyzed.

Liquid assisted grinding (LAG) was performed with a Retsch MM 400 Mixer Mill, equipped with two grinding jars in which five 2mL Eppendorf tubes can be installed. Typically, 0.2 mmol of Nefiracetam is added to an Eppendorf, as well as 4 stainless steel beads and 10µl of solvent. The milling program is set for 90 minutes at 30Hz.

Slurrying experiments were performed by preparing Nefiracetam suspensions in selected solvents at 25°C. The vials are sealed and the suspension left over 5 days at 25°C under a stirring of 700 rpm using a Cooling Thermomixer HLC. Solid phases were then retrieved and analyzed.

Methods

Suitable crystals of Nefiracetam FI, FII and monohydrate were analyzed using Single-Crystal X-Ray diffraction (SCXRD) with data measured on a "Rigaku Ultra X18S generator, FOX3D mirrors". The diffracted beams are detected by a "Mar345 image plate" using a MoKα (λ = 0.71 Å). Images have been integrated by "CrysalisPro".

Single crystal X-Ray diffraction data for Nefiracetam **FIII** was collected on an Oxford Diffracton Gemini R Ultra diffractometer (Ruby CCD detector using CuKα radiation). Data reduction was carried out using the CrystAlisPro software package[27]. The resolution and the refinement by full-matrix least squares have been done using respectively SHELXT and SHELX-2014/7[28]. Non-hydrogen atoms were refined anisotropically; H-atoms is added in calculated positions and allowed to ride on the parent atoms, with isotropic displacement factors set to 1.2 Ueq of the parent atoms (Uiso (H)= 1.5 Ueq (C) for methyl). The H-atoms of the methyl groups were allowed to undergo free rotation about the local threefold axis. Symmetry analysis and validation were carried out using PLATON[29]. Pictures were made using the molecular visualization software Mercury[30].

Powder X-Ray Diffraction (XRPD) data were collected on a PANalytical Bragg-Brentano diffractometer, using Ni-filtered CuKα (λ = 1.54179 Å) at 45 kV and 30 mA with a X'Celerator detector. Each sample was analyzed between 4 and 40° in 2θ with a step size of ca. 0.0167° and a total scan time of 6min42s. Regarding the non-ambient XRPD measurement (VT-XRPD), samples were heated using an "Anton Paar TTK-450" heating device and isotherms (15 minutes) were applied between each temperature step.

Differential Scanning Calorimetry (DSC) measurements were performed from 30 to 175°C at a scanning rate of 5°C/min on a "Mettler Toledo DSC821e". Solid samples (weight of 6-7mg) were placed in an aluminum crucible with pierced sealed lids and nitrogen was used as purge gas with a flow rate of 50mL/min. Indium is used as a reference. Heats of fusion were extracted from thermograms obtained between 30 and 175°C at a scanning rate of 2°C/min on a "TA instrument DSC2500".

Thermogravimetric analysis (TGA) was performed from 30 to 400°C at a scanning rate of 10°C/min on a "Mettler Toledo TGA-STDA 851e". Solid samples (weight of 6-7mg) were placed in aluminum oxide crucible and nitrogen was used as purge gas with a flow rate of 50mL/min.

Humidity exposure experiments have been performed storing Nefiracetam samples at 18°C and 100% RH for different time ranges.

Calibration lines for High Performance Liquid Chromatography (HPLC) were first built in order to dose the Nefiracetam by correlating the area under the curve (AUC) and the concentration prepared with a linear equation. Nefiracetam samples were first diluted 1000x using an acetonitrile 1:1 water MilliQ (in volume) diluent. Nefiracetam concentrations were dosed using the following HPLC parameters: Device: Waters Alliance 2695; Column: Waters Sunfire C18, 4.6x100 mm, 3.5 µm; Detector : PDA 2998 (extraction at λ = 210 nm); T° = 40°C; Injection volume: 10 µL; Flow : 1.2 mL/min; Mobile phase A : H_2O + 0,1% H_3PO_4; Mobile Phase B : CH_3CN + 0,1% H_3PO_4; Gradient :0 min → 30 % B; 0.5 min → 30 % B; 4.5 min → 90 % B; 6.5 min → 90 % B; Stop time: 15 min.

Concerning dissolution experiments, **FI** and monohydrate were previously ground using mortar and pestle to get approximately the same particle size range. Supersaturated Nefiracetam **FI** and monohydrate solution in 50mL of solvent at 0°C and 10°C were prepared in a 100mL flask using an "EasyMax 102 Advanced Synthesis Workstation" (manufactured by Mettler Toledo) equipped with a mechanical 150 rpm stirring and a temperature monitor. The Nefiracetam IR signature in solution is recorded from 2800 cm^{-1} to 650 cm^{-1} every 15 seconds (50 scans) until the equilibrium using an online "React IR iC 10" by Mettler Toledo AutoChem with a 6.5 mm AgX DiComp Fiber Conduit probe as ATR crystal coupled to the crystallization reactor. ReactIR data are monitored with the iC IR software. The normalized IR intensities are then converted into molar concentration using the thermodynamic solubility determined by HPLC measurement.

RESULTS AND DISCUSSION

Form screening

A form screen (**Table 1**) was performed using evaporative, slurrying and cooling crystallization experiments (with 12 different solvents), grinding experiments, as well as crystallization experiments from the melt, and heating of solids. XRPD analysis was performed on each sample to identify the crystal form. Evaporation and cooling experiments in organic solvents always led to the formation of **FI** which is the form described by Wang et al.[26] However in water, we identified a so far unknown monohydrate of Nefiracetam, both from the solvent evaporation as well as cooling crystallization experiment. Extended humidity exposure of **FI** (3-5 days at 100% RH) led also to the monohydrate formation. Once the monohydrate is formed, it remains stable over a long period of time (one week) under ambient temperature, pressure and relative humidity conditions. Traces of this form were also present when using, hygroscopic organic solvents such as alcohols. Surprisingly, when heating **FI** a transition to a second polymorph of Nefiracetam (**FII**) occurred at temperatures above 135-145°C temperature. This solid-solid transition is clearly visible in the VT-XRPD experiments (**Figure 5**). Upon crystallization of the melt, a third polymorph (**FIII**) was observed. XRPD patterns clearly allow distinguishing the four solid forms of Nefiracetam (**Figure 2**).

Table 1 : Form screening performed on the Nefiracetam and the relative solid forms observed in XRPD

Solvent	Crystallization method	Crystal form (XRPD)
Organic solvents*	Evaporation	**FI**
	Cooling	**FI**
	Grinding (LAG)	**FI**
	Slurrying	**FI**
Water	Evaporation	Monohydrate
	Cooling	Monohydrate
	Grinding (LAG)	Monohydrate
	Slurrying	Monohydrate
/	From the melt	**FIII**
/	Δ 135°C	**FII**

*Ethylacetate, methylacetate, ethanol, methanol, 2-propanol, tetrahydrofuran, acetonitrile, toluene, acetone, chloroform and dichloromethane

Structural analysis

To investigate the structural differences between the different forms, single-crystals of each form were grown. Nefiracetam **FI** was obtained in organic solvents by evaporative and cooling crystallizations. The structure refined is identical to the one described by Wang et al[26]. Single crystals of the monohydrate were grown from water. **FII** single crystals were prepared by heating a single crystal of Nefiracetam **FI** to 135-145°C and holding it there for 1h. This crystal was then quenched at room temperature and analyzed. This procedure needed to be repeated on a number of crystals to achieve a sufficient amount of diffraction data, as the single crystals of **FII** inherently reverted back to **FI** in a single crystal to single crystal transition. Concerning the third polymorphic form **FIII**, suitable single crystals were obtained from the melt, allowing this latter to cool to room temperature. As for the second polymorph, transition to **FI** ultimately occurred, so that the data set needed to be acquired over multiple samples in order to get sufficient diffraction data.

The simulated XRPD patterns overlap with the experimentally determined ones (**Figure 2**). **Table 2** summarizes all single crystal data.

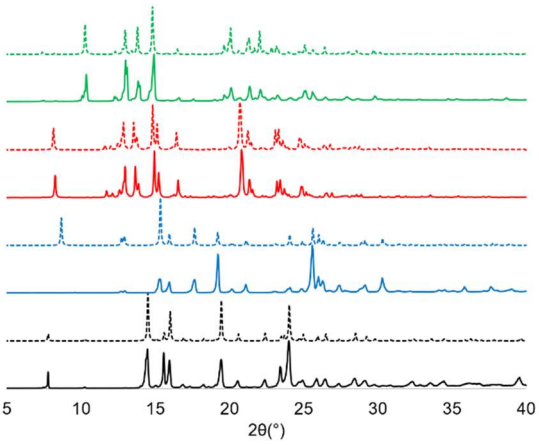

Figure 2: Simulated diffraction patterns (dashed line) of all Nefiracetam solid forms and comparison with the experimental ones (full line); Nefiracetam **FIII** (green), Nefiracetam **FII** (red), Nefiracetam **FI** (black) and Nefiracetam **monohydrate** (blue).

FI crystallizes in the orthorhombic $P2_12_12_1$ space group. Its crystal packing shows Nefiracetam molecules in a stacked arrangement built up by intermolecular hydrogen bonds leading to a $C_1^1(4)$ pattern according to the Etter's graph notation[31-32] along the b-axis (**Figure 3a**). The hydrogen bond (N_1-$H_1\cdots O_1$) involves the N-H group of the amide and the carbonyl group of the amide of a second molecule. In addition to this hydrogen bond, only dispersive interactions guide the molecule organization of this crystal structure and no π-stacking is observed. Nefiracetam **FII** crystallizes in the triclinic *P*-1 space group and the lattice clusters 12 molecules that display 6 non-equivalent amide-amide hydrogen bonds in the crystal structure. These hydrogen bonds form chains along the a-axis stacking the molecules in this direction as illustrated in **Figure 3c**. Values of distance and angle related to each intermolecular hydrogen bond are resumed in the Supporting Information. The third anhydrate **FIII** crystallizes in the monoclinic $P2_1/n$ space group and the lattice clusters 8 molecules wherein two non-equivalent hydrogen bonds lead the structural arrangement similar to the two other anhydrous forms, with parallel chains appearing along the a-axis **(Figure 3e)**. Both **FII** and **FIII** display the same $C_2^2(8)$ hydrogen bond network, and a less dense crystalline lattice, compared to **FI**. Finally, the monohydrate is disordered around the pyrrolidone ring with only one orientation shown here for clarity. The hydrate crystallizes in the monoclinic *Pc* space group. In this structure, there are no intermolecular hydrogen bonds between two racetam molecules. Instead, water occupies sites between Nefiracetam molecules and water hydrogens form an O-H···O hydrogen bond with the amide carbonyl group of a first Nefiracetam molecule and an O-H···O hydrogen bond with the pyrrolidone carbonyl group of a second. Furthermore, the water oxygen atom interacts with the N-H group of the amide of a third Nefiracetam molecule in a N-H···O bond. This leads to an extending $C_4^4(18)$ chain **(Figure 3g)** and reflects in a dense packing 1.26 $g.cm^{-3}$ compared to 1.220 (**FI**), 1.205 (**FII**), 1.152 $g.cm^{-3}$ (**FIII**) for the three anhydrate forms.

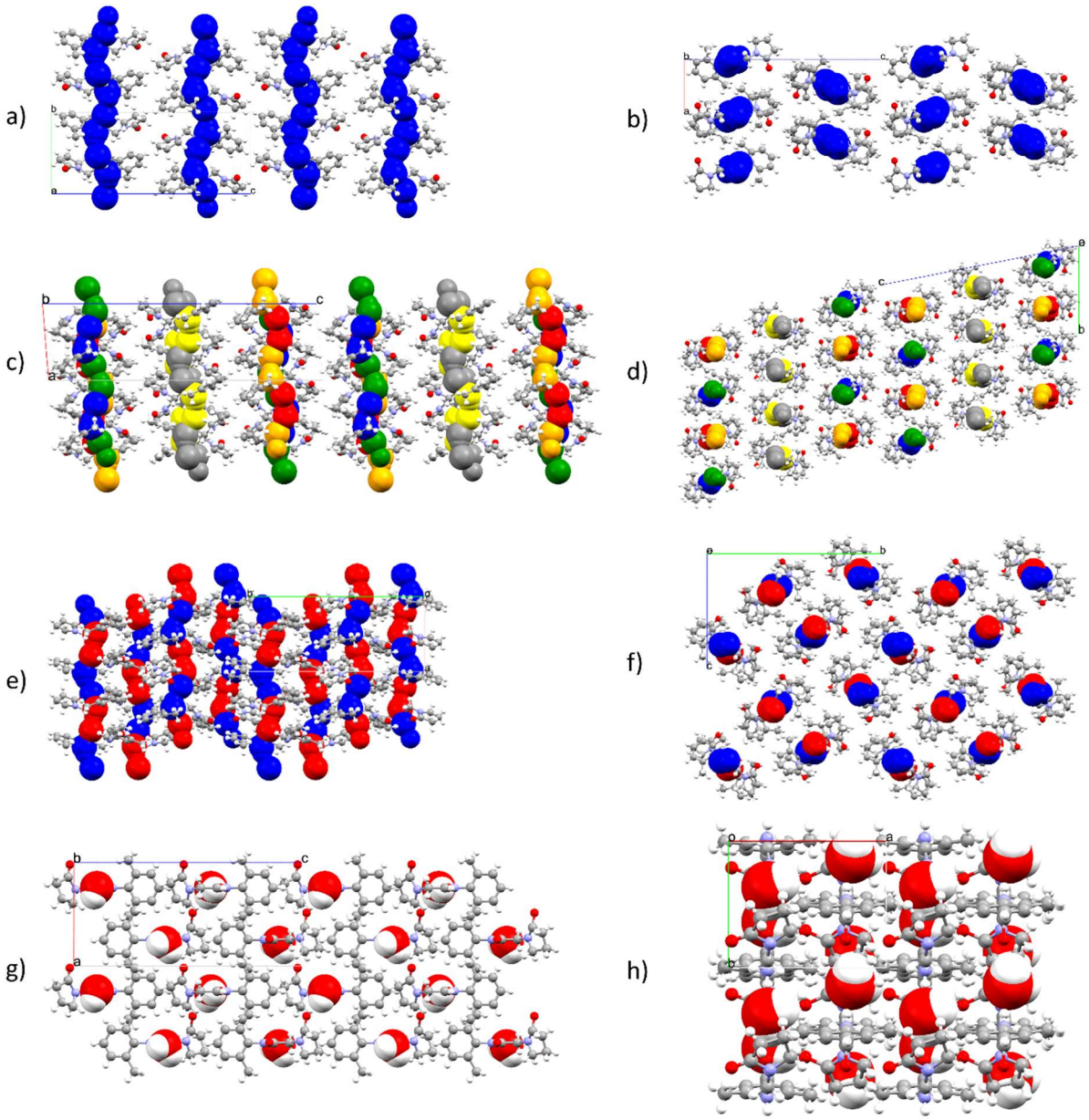

Figure 3: Molecular arrangements in crystalline a) Nefiracetam Form I along the a-axis, b) Nefiracetam Form I along the b-axis, c) Nefiracetam Form II along the c-axis d) Nefiracetam Form II along the a-axis, e) Nefiracetam Form III along the b-axis, f) Nefiracetam Form III along the a-axis, g) Nefiracetam monohydrate along the b-axis and h) Nefiracetam monohydrate along the c-axis. Regarding the anhydrous forms, hydrogen bonds (D-H⋯A) are highlighted using colored spacefill representation. Each spacefill color represents a non-equivalent amide-amide hydrogen bond. In case of the monohydrate, water is underlined using spacefill also

Table 2: Main crystallographic data of all four solid forms of Nefiracetam and refinement parameters

Compound	**Nefiracetam FII**	**Nefiracetam FIII**	**Nefiracetam monohydrate**
Empirical formula	$C_{14}H_{18}N_2O_2$	$C_{14}H_{18}N_2O_2$	$C_{14}H_{18}N_2O_2.H_2O$
Formula weight (g/mol)	246.30	246.30	264.32
Temperature (K)	293(2)	297(2)	293(2)
Wavelength (Å)	0.71073	0.71073	0.71073
Crystal system	Triclinic	Monoclinic	Monoclinic
Space group	*P*-1	$P2_1/n$	*Pc*
a, b, c (Å)	9.0237(16),14.0397(13),32.872(6)	9.1823(10),21.497(3),14.624(2)	9.2368(7),7.3939(4),20.3969(14
α, β, γ (°)	78.835(12),85.365(15),89.403(11)	90,100.267(14),90	90,90.039,90
Volume ($Å^3$)	4072.3(11)	2840.5(6)	1393.02 (17)
Z	12	8	4
Density calculated (mg/m^3)	1.205	1.152	1.260
Absorption coefficient (mm^{-1})	0.081	0.078	0.089 mm^{-1}
F(000)	1584	1056	568
Crystal size			0.35 x 0.30 x 0.20 mm^3
Theta range for data collection(°)	2.837 to 18.845	2.439 to 23.292	2.930 to 25.342
Reflections collected	9338	7989	8904
Independent reflections	5819 [R(int) = 0.1479]	3908 [R(int) = 0.0776]	4796 [R(int) = 0.0371]
Completeness to theta = 25.96°	90.9%	95.3%	99.0 %
Absorption correction			Semi-empirical from equivalents
Max. and min. transmission			1.00000 and 0.78721
Data / restraints / parameters	5819 / 648 / 985	3908 / 136 / 373	4796 / 198 / 476
Goodness-of-fit on F^2	0.864	1..092	1.076
Final R indices [I>2sigma(I)]	R1 = 0.0925, wR2 = 0.1138	R1 = 0.0906, wR2 = 0.2227	R1 = 0.0662, wR2 = 0.1588
R indices (all data)	R1 = 0.2926, wR2 = 0.1556	R1 = 0.1633, wR2 = 0.2864	R1 = 0.0836, wR2 = 0.1700
Extinction coefficient		n/a	n/a
Largest diff. peak and hole ($e.Å^{-3}$)	0.136 and -0.153	0.370 and -0.270	0.182 and -0.197

Stability relationship between the different forms

TGA data (**Figure 4**) shows Nefiracetam to be stable up to 280°C, temperature at which degradation occurs. The hydrate form shows a supplementary weight loss between 60°C and 100°C corresponding to the loss of one equivalent of water (the experimental weight loss (7%) fits the theoretical one (6.8%)).

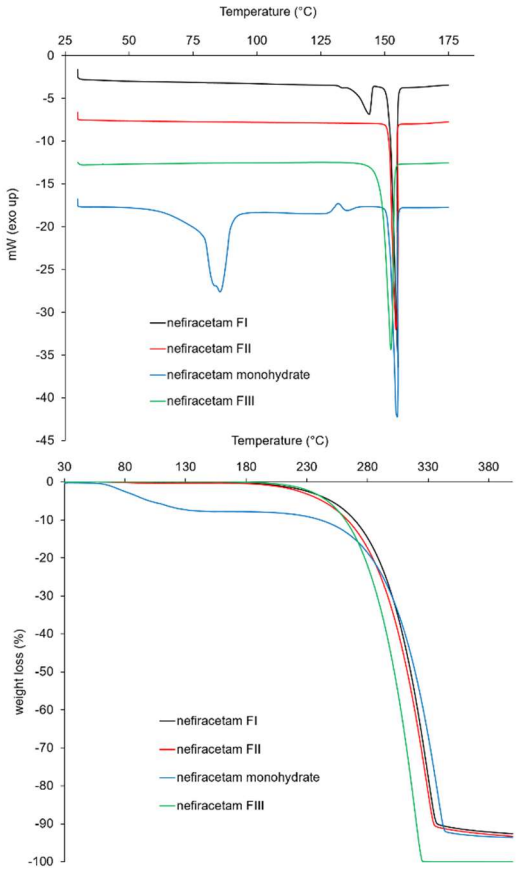

Figure 4: DSC (above) and TGA (below) curves of all four solid forms of Nefiracetam .

Upon heating, **FII** shows a single melting endotherm at 150°C. When heating **FI**, two successive endotherms can be observed, a first around 140°C corresponds to the melting of **FI** combined with a recrystallization exotherm of **FII** and a second corresponding to the melting of **FII**. The VT-PXRD performed on Nefiracetam **FI** highlights a similar behavior with **FI** remaining stable up to 135°C where a **FI** to **FII** transition occurs. Nefiracetam **FII** reverts back to **FI** within 2 days at room temperature. These results thus show an enantiotropic relationship between both forms.

FIII spontaneously recrystallizes from the melt if the cooling rate is low enough (2°C/min or less). Rapid cooling rates lead to an amorphous phase. When heating **FIII** in the DSC device, a melting endotherm overlapping the **FII** melting (150°C) endotherm is observed. This could be due to **FII** and **FIII** having close lying melting points, or to an *in situ* solid-solid transformations occurring upon heating. Indeed, this form is only short lived, as it completely reverts to **FI** within 16hrs at 25°C as shown by XRPD. VT-XRPD highlights the **FIII** to **FI** conversion starting at 50-60°C and suggests that the metastable form tends to rapidly transform at high temperature. DSC experiments

performed on **FIII**, on the other hand, do not display such a conversion into **FI** but a direct transformation into **FII)**. VT-XRPD of the hydrate (**Figure 5**) aligns with the DSC and TGA data, showing a dehydration at around 80°C. After this loss of crystalline water, **FI** is observed (VT-XRPD), which aligns with the DSC measurement showing an endothermic event at around 135°C attributed to the **FI-FII** solid-solid transition.

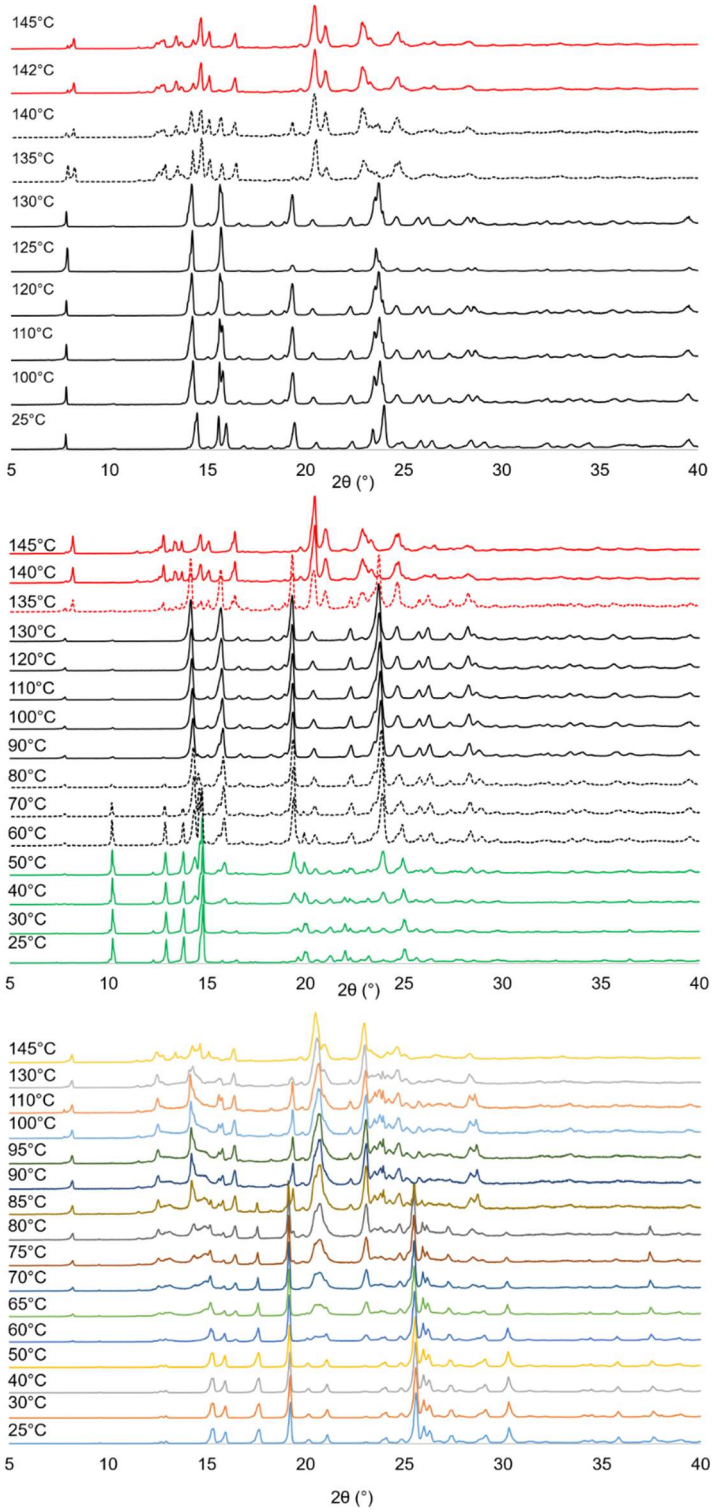

Figure 5: VT-XRPD pattern of FI (above), FIII (middle) and monohydrate (below). Nefiracetam FI, FII, FIII and monohydrate patterns are highlighted using a color code which is black (FI), red (FII), green (FIII) and blue (monohydrate). The related dashed line highlights mixture of two forms.

In a summary, **Figure 6** highlights the transitions observed in this contribution between all solid forms of Nefiracetam.

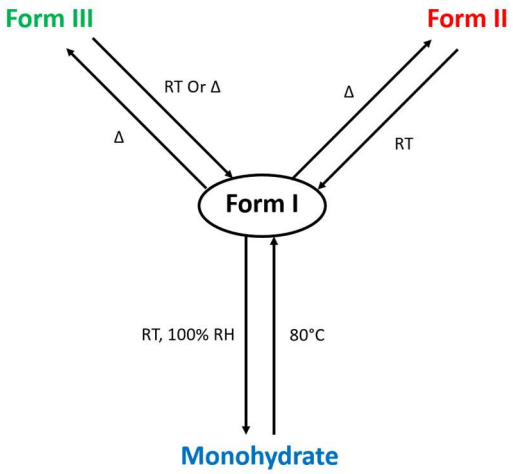

Figure 6: Transitions between Nefiracetam crystalline forms

FI is clearly the most stable form at ambient temperature, which is also in alignment with the more dense packing of this form. **FII** and **FI** were found to be enantiotropically[33] related. A transition point exists before the melting point of **FI** (140°C), with **FI** being stable below this transition point and **FII** above this temperature. The enantiotropic relationship between **FI** and **FII** is also confirmed by the heat of fusion rule. The heat of melting of **FI** ($\Delta H_{m,FI}$) has been measured integrating the total heat exchanges prior to the onset of melting of **FI** up to total fusion of **FII** (starting with a solid phase **FI** up to a liquid phase). Values of -117.78 $J.g^{-1}$ (-29.0 $kJ.mol^{-1}$) and -91.05 $J.g^{-1}$(-22.43 $kJ.mol^{-1}$) are obtained respectively for $\Delta H_{m,FI}$ and $\Delta H_{m,FII}$. Since **FII** has a higher melting point, this indeed aligns with Burger's Heat of Fusion Rule (HFR)[34-35] for an enantiotropic system, showing the system with the highest melting point to have the lowest heat of fusion. **Figure 7** represents this schematically. **FIII** is identified as a meta-stable polymorph, which transforms rapidly into **FI** at room temperature or alternatively into **FII** upon heating.

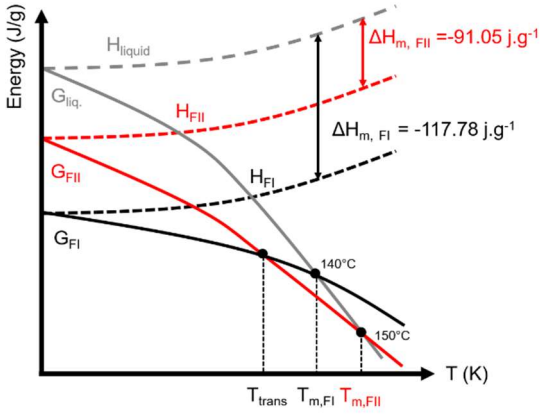

Figure 7: Energetic diagram in case of enantiotropic system.

Dissolution profile of the Nefiracetam solid forms in organic solvent

Figure 8 shows the dissolution curves of **FI** and monohydrate in ethanol and acetonitrile
.

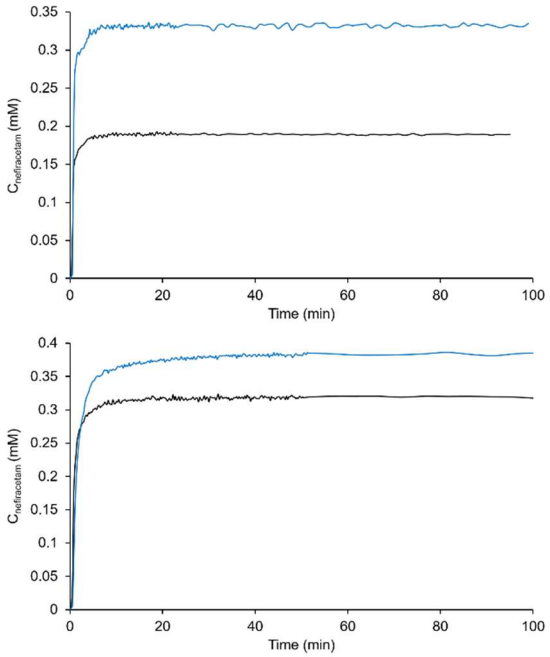

Figure 8: *Dissolution curve of Nefiracetam FI and monohydrate in (above) acetonitrile at 10°C and (below) ethanol 0°C. The concentration of Nefiracetam in solution is recorded overtime.*

Both solvents show a rapid dissolution of both forms, with solubility being reached in the first five minutes. In both solvents, the hydrate displays a significant solubility improvement. In ethanol, the Nefiracetam **FI** solubility at the equilibrium is about 0.32 mM and about 0.40 mM using the monohydrate as solid form. However, this improvement appears to be stronger in acetonitrile where the solubility increases from 0.19 mM to 0.34 mM. Such a difference could be explained due to the difference in water activity which is solvent dependent. No solid transition between **FI** to/from the hydrate was observed in the 2h time-laps of the experiment. For the metastable form (**FIII**), it was not possible to determine the "apparent" or "kinetic" solubility [36-37], as the solvent-mediated conversion into the most stable form occurs too rapidly. As **FII** is only observable at high temperature, its dissolution behavior could not be evaluated.

CONCLUSION

Solid forms of the anti-dementia agent Nefiracetam have been fully screened by evaporative, cooling, slurrying, grinding and melt crystallization methods. Three novel solid-state forms of Nefiracetam have been discovered: a second and a third anhydrous polymorph as well as a monohydrate. All the solid forms have been structurally and thermally analyzed their respective stability evaluated. An enantiotropic relationship between the stable polymorph (**FI**) at room temperature and the other two forms (**FII** and **FIII**) has been highlighted. Since, the solid-solid transition between the **FI** and **FII** forms occurs at high temperature and Nefiracetam **FIII** only exists for a few hours after recrystallization from the melt, Nefiracetam **FI** as well as the hydrated form appear as interesting candidates for formulation purposes. Long-term exposure (about 3 days) of

FI at 100% RH reveals the formation of monohydrate with the monohydrate remaining stable at least for one week under ambient conditions. Dissolution experiments performed on the Nefiracetam monohydrate solid form have shown that a hydrate form significantly improves the solubility in organic solvents. So given the appropriate formulation conditions this drug shows a case where two different solid forms could potentially successfully be marketed.

ASSOCIATED CONTENT

ACKNOWLEDGMENTS

Authors are greatly thankful to Dr. Andrea Carletta for the relevant advices and interest in this work. Authors also thank Laurent Collard for the HPLC set-up assistance. This article was published due to financial support from the "Fonds Européen de Développement Régional" (FEDER) and the "Wallonie".

AUTHOR INFORMATION

*e-mail: xavier.buol@uclouvain.be. Tel : +32 (0)475 92 57 98

*e-mail : tom.leyssens@uclouvain.be.

CONFLICTS OF INTEREST

There is no conflict to declare.

REFERENCE

1. Watabe, S.; Yamaguchi, H.; Ashida, S.-i., DM-9384, a new cognition-enhancing agent, increases the turnover of components of the GABAergic system in the rat cerebral cortex. *European journal of pharmacology* **1993,** *238* (2-3), 303-309.
2. Otomo, E.; Takasu, Y.; Shiotani, T.; Hasegawa, K.; Honma, A., Agent for improving dementia. Google Patents: 1999.
3. Otomo, E.; Takasu, Y., Use of Nefiracetam for treating neurodegeneration. Google Patents: 2004.
4. Hirata, K.; Katayama, S.; Yamazaki, K.; Fujikane, M.; Katayama, K., Electric field distribution of event-related potentials in stroke patients. *Brain topography* **1996,** *8* (3), 279-284.
5. Crespi, F., Nefiracetam. Daiichi Seiyaku. *Current opinion in investigational drugs (London, England: 2000)* **2002,** *3* (5), 788-793.
6. Yoshii, M.; Watabe, S., Enhancement of neuronal calcium channel currents by the nootropic agent, Nefiracetam (DM-9384), in NG108-15 cells. *Brain research* **1994,** *642* (1-2), 123-131.
7. Shimomura, K.; Shimada, M.; Hagiwara, M.; Harada, S.; Kato, M.; Furuhama, K., Testicular toxicity induced in dogs by Nefiracetam, a neutrotransmission enhancer. *Reproductive Toxicology* **2004,** *18* (3), 423-430.
8. Nabeshima, T.; Tohyama, K.; Murase, K.; Ishihara, S.-i.; Kameyama, T.; Yamasaki, T.; Hatanaka, S.; Kojima, H.; Sakurai, T.; Takasu, Y., Effects of DM-9384, a cyclic derivative of GABA, on amnesia and decreases in GABAA and muscarinic receptors induced by cycloheximide. *Journal of Pharmacology and Experimental Therapeutics* **1991,** *257* (1), 271-275.

9. Suliman, N. A.; Taib, M.; Norma, C.; Moklas, M.; Aris, M.; Adenan, M. I.; Hidayat Baharuldin, M. T.; Basir, R., Establishing natural nootropics: recent molecular enhancement influenced by natural nootropic. *Evidence-Based Complementary and Alternative Medicine* **2016,** *2016*.
10. Shimada, H.; Hattori, C.; Tanaka, N.; Takayama, S., Mutagenicity study of the new cognition-enhancing agent Nefiracetam. *Arzneimittel-Forschung* **1994,** *44* (2A), 251-253.
11. Wagai, N.; Yamaguchi, F.; Hasegawa, T.; Takayama, S., Antigenicity study of the new cognition-enhancing agent Nefiracetam. *Arzneimittel-Forschung* **1994,** *44* (2A), 247-250.
12. Watanabe, T.; Matsuhashi, K.; Shimada, M.; Harada, S.; Tawara, K.; Takayama, S., Reproductive toxicity studies of the new cognition-enhancing agent Nefiracetam in rats and rabbits. *Arzneimittel-Forschung* **1994,** *44* (2A), 239-242.
13. Kawabata, Y.; Wada, K.; Nakatani, M.; Yamada, S.; Onoue, S., Formulation design for poorly water-soluble drugs based on biopharmaceutics classification system: basic approaches and practical applications. *International journal of pharmaceutics* **2011,** *420* (1), 1-10.
14. Di, L.; Fish, P. V.; Mano, T., Bridging solubility between drug discovery and development. *Drug Discovery Today* **2012,** *17* (9-10), 486-495.
15. Amidon, G. L.; Lennernäs, H.; Shah, V. P.; Crison, J. R., A theoretical basis for a biopharmaceutic drug classification: the correlation of in vitro drug product dissolution and in vivo bioavailability. *Pharmaceutical research* **1995,** *12* (3), 413-420.
16. Ku, M. S., Use of the biopharmaceutical classification system in early drug development. *The AAPS journal* **2008,** *10* (1), 208-212.
17. Savjani, K. T.; Gajjar, A. K.; Savjani, J. K., Drug solubility: importance and enhancement techniques. *ISRN pharmaceutics* **2012,** *2012*.
18. Dokoumetzidis, A.; Macheras, P., A century of dissolution research: from Noyes and Whitney to the biopharmaceutics classification system. *International journal of pharmaceutics* **2006,** *321* (1-2), 1-11.
19. Gardner, C. R.; Walsh, C. T.; Almarsson, Ö., Drugs as materials: valuing physical form in drug discovery. *Nature Reviews Drug Discovery* **2004,** *3* (11), 926.
20. Chen, J.; Sarma, B.; Evans, J. M.; Myerson, A. S., Pharmaceutical crystallization. *Crystal growth & design* **2011,** *11* (4), 887-895.
21. Elder, D. P.; Holm, R.; de Diego, H. L., Use of pharmaceutical salts and cocrystals to address the issue of poor solubility. *International journal of pharmaceutics* **2013,** *453* (1), 88-100.
22. Morissette, S. L.; Almarsson, Ö.; Peterson, M. L.; Remenar, J. F.; Read, M. J.; Lemmo, A. V.; Ellis, S.; Cima, M. J.; Gardner, C. R., High-throughput crystallization: polymorphs, salts, co-crystals and solvates of pharmaceutical solids. *Advanced drug delivery reviews* **2004,** *56* (3), 275-300.
23. Serajuddin, A. T., Salt formation to improve drug solubility. *Advanced drug delivery reviews* **2007,** *59* (7), 603-616.
24. Thipparaboina, R.; Kumar, D.; Chavan, R. B.; Shastri, N. R., Multidrug co-crystals: towards the development of effective therapeutic hybrids. *Drug Discovery Today* **2016,** *21* (3), 481-490.
25. Wouters, J.; Quéré, L., *Pharmaceutical salts and co-crystals*. Royal Society of Chemistry: 2011.
26. Wang, P.-L.; Wang, H.-B.; Ding, W.-L.; Liu, Z.-Q.; Xing, Z.-T., N-(2, 6-Dimethylphenyl)-2-(2-oxo-1-pyrrolidin-1-yl) acetamide. *Acta Crystallographica Section E: Structure Reports Online* **2006,** *62* (9), o3838-o3839.
27. Rigaku, O. D., CrysAlisPro Software System, Version 1.171. 38.41 l, Rigaku Coorporation. Oxford, UK: 2015.
28. Sheldrick, G. M., Crystal structure refinement with SHELXL. *Acta Crystallographica Section C: Structural Chemistry* **2015,** *71* (1), 3-8.
29. Spek, A. L., Structure validation in chemical crystallography. *Acta Crystallographica Section D: Biological Crystallography* **2009,** *65* (2), 148-155.

30. Macrae, C. F.; Bruno, I. J.; Chisholm, J. A.; Edgington, P. R.; McCabe, P.; Pidcock, E.; Rodriguez-Monge, L.; Taylor, R.; Streek, J. v. d.; Wood, P. A., Mercury CSD 2.0–new features for the visualization and investigation of crystal structures. *Journal of Applied Crystallography* **2008,** *41* (2), 466-470.
31. Etter, M. C.; MacDonald, J. C.; Bernstein, J., Graph-set analysis of hydrogen-bond patterns in organic crystals. *Acta Crystallographica Section B* **1990,** *46* (2), 256-262.
32. Bernstein, J.; Davis, R. E.; Shimoni, L.; Chang, N. L., Patterns in hydrogen bonding: functionality and graph set analysis in crystals. *Angewandte Chemie International Edition in English* **1995,** *34* (15), 1555-1573.
33. Park, K.; Evans, J. M.; Myerson, A. S., Determination of solubility of polymorphs using differential scanning calorimetry. *Crystal Growth & Design* **2003,** *3* (6), 991-995.
34. Burger, A.; Ramberger, R., On the polymorphism of pharmaceuticals and other molecular crystals. I. *Microchimica Acta* **1979,** *72* (3-4), 259-271.
35. Burger, A.; Ramberger, R., On the polymorphism of pharmaceuticals and other molecular crystals. II. *Microchimica Acta* **1979,** *72* (3-4), 273-316.
36. Nicoud, L.; Licordari, F.; Myerson, A. S., Estimation of the Solubility of Metastable Polymorphs: A Critical Review. *Crystal Growth & Design* **2018,** *18* (11), 7228-7237.
37. Nicoud, L.; Licordari, F.; Myerson, A. S., Polymorph control in batch seeded crystallizers. A case study with paracetamol. *CrystEngComm* **2019**.